Anisotropy of flow and the order of phase transition in relativistic heavy ion collisions

Pasi Huovinen

Helsinki Institute of Physics, P.O. Box 64, FIN-00014 University of Helsinki, Finland
and
Department of Physics, P.O. Box 35, FIN-40014 University of Jyväskylä, Finland

Abstract

Using a hydrodynamical model we study how the order of phase transition in the equation of state of strongly interacting matter affects single particle spectra, elliptic flow and higher order anisotropies in Au+Au collisions at RHIC ($\sqrt{s_{\mathrm{NN}}} = 200$ GeV energy). We find that the single particle spectra are independent of the order of phase transition and that the fourth harmonic $v_4(p_T)$ shows only a weak dependence in the p_T region where hydrodynamics is expected to work. The differential elliptic flow, $v_2(p_T)$, of baryons shows the strongest dependence on equation of state. Surprisingly the closest fit to data was obtained when the equation of state had a strong first order phase transition and a lattice inspired equation of state fits the data as badly as a purely hadronic equation of state.

Key words: relativistic heavy ion collisions, elliptic flow, order of phase transition, hydrodynamic model
PACS: 25.75.-q, 25.75.Ld, 25.75.Nq

1 Introduction

In non-central heavy ion collisions at the Relativistic Heavy Ion Collider (RHIC) of BNL the particle distributions exhibit quite large anisotropies [1,2,3]. The second Fourier coefficient of the azimuthal distribution of particles, so called elliptic flow, has been extensively studied [4] since it is sensitive to the early dense stage of the evolution [5]. Recently also higher harmonics have been

Email address: `pasi.huovinen@phys.jyu.fi` (Pasi Huovinen).

measured [3,6]. It has been claimed that they should be even more sensitive to the initial configuration of the system [7].

Ideal fluid hydrodynamics has been particularly successful in describing the observed anisotropy of particles at low p_T in minimum bias collisions [8,9]. This success has been interpreted as a sign of formation of thermalized matter rapidly after the primary collision [10]. Studies of both single particle spectra and anisotropies have also shown that a reasonable reproduction of data favours an Equation of State (EoS) of strongly interacting matter with a phase transition [11,12].

The lattice QCD calculations of the EoS of strongly interacting matter support such a scenario by predicting a phase transition at $T_c \approx 170$ MeV temperature. For a physical scenario of two light and one heavier quark, the phase transition is predicted to be a smooth crossover at small values of baryochemical potential. Contrary to naive expectations, lattice QCD predicts that pressure and energy density do not reach their ideal Stefan-Boltzmann values immediately above the critical temperature, but approach them slowly [13].

At mid-rapidity at collisions at RHIC, the net baryon density is small and the relevant EoS should exhibit a crossover transition. However, so far all hydrodynamical calculations of elliptic flow [10,11,12,14,15,16,17,18,19] have used an EoS with a strong first order phase transition and ideal parton gas to describe the plasma phase. The usual point of view has been that it is unlikely that the details of phase transition would lead to significant dynamical effects [9]. This standpoint has been supported by the early calculations [20,21] where it was found that the width of the phase transition region, ΔT, had only little effect on the final flow pattern in one dimensional flow. Thus it was considered safe to claim that the final particle distributions would not be sensitive to ΔT either.

However, full three dimensional expansion is more complicated than one dimensional. It is known that in three dimensional expansion the differential elliptic anisotropy, $v_2(p_T)$, of (anti)protons is sensitive to the existence of phase transition and its latent heat [11,12,15]. The anisotropy of flow might thus be sensitive to other details of phase transition as well. In this paper we address this possible sensitivity. We use a hydrodynamical model to calculate single particle spectra, elliptic flow and higher order anisotropies in $\sqrt{s_{NN}} = 200$ GeV Au+Au collisions using four different EoSs with different phase transitions and plasma properties. As a representative of lattice QCD results, we use an EoS based on the thermal quasiparticle model of Schneider and Weise [22] (EoS qp). This model is tuned to reproduce the lattice QCD EoS and provides a method to extrapolate the results to physical quark masses. To facilitate comparison with earlier calculations we use as reference points the EoSs Q and H used in Refs. [10,12,14,15,16]. EoS Q has a first order phase transition

between hadron gas and an ideal parton gas whereas EoS H is a hadron gas EoS without any phase transition. To study the effects of the order of phase transition and slow approach to the Stefan-Boltzmann limits separately we also use a simple parametrisation for an EoS (EoS T) where the hadron gas and ideal parton gas phases are connected using a hyperbolic tangent function. Such an EoS has a smooth crossover transition but the plasma properties approach their ideal values much faster than in EoS qp.

We find that the main sensitivity to the details of an EoS lies in the differential elliptic flow of heavy particles ($m \gtrsim 1$ GeV) where EoS Q with a first order phase transition leads to an anisotropy closest to the data. Surprisingly, the lattice inspired EoS qp reproduces the data as badly as purely hadronic EoS. EoS T with a crossover transition leads to almost as good results as EoS Q. Thus hydrodynamical description of elliptic flow does not require a strong first order phase transition, but it does require sufficiently large increase in entropy and energy densities within sufficiently small temperature interval.

2   Equation of State

Until recently the lattice QCD calculations were restricted to vanishing net baryon densities, $\mu_B = 0$. Even if there are some recent results for $\mu_B \neq 0$ [13], we limit our discussion to zero net baryon density for the sake of simplicity. Since we are interested in the behaviour of the collision system at midrapidity at RHIC where net baryon density is small, this approximation is unlikely to cause a large effect. Thermal models suggest that around phase transition temperature, the baryon chemical potential is below 50 MeV [23] corresponding to a quark chemical potential of about 15 MeV. At these small values of μ the critical temperature is expected to change by less than a percent from that at $\mu = 0$ [13]. One of our EoSs (EoS Q, see below) also includes extension to non-zero baryon densities. We have checked that for this EoS, the results obtained when the finite baryon density is included in the EoS or approximated by zero, differ by less than two percents. Even if we do not include finite baryon density to the EoS, we still have finite baryon current in our hydrodynamical calculation. This allows us to have different baryon and anti-baryon yields at freeze-out and thus finite net proton yields.

So far the lattice QCD calculations with quarks must be done using unphysically large quark masses. The calculated equation of state must therefore be extrapolated to physical quark mass values. For this purpose we use the thermal quasiparticle model of Schneider and Weise [22]. In this model the lattice QCD results are described in terms of quasiparticles with temperature dependent effective masses and effective number of degrees of freedom. In this approach the EoSs obtained in lattice calculations for pure glue [24] and dif-
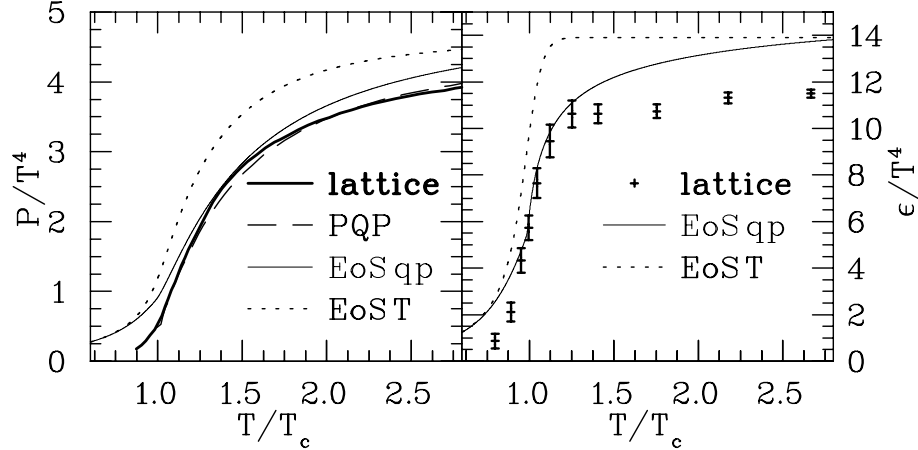
Fig. 1. The lattice results for pressure (left panel) and energy density (right panel) [25] compared to the quasiparticle model with quark masses as used in the lattice calculation (PQP), quasiparticle model with physical quark masses (EoS qp) and a parametrized EoS T (introduced later in the text). The lattice result for pressure is extrapolated to continuum limit by $p_{cont} \approx 1.1 p_{lat}$ [22].

ferent number of quark flavours [25] are well reproduced. Since the mass of quarks is an explicit parameter in this model, it is easy to extrapolate the results to physical quark masses. Here we use the quasiparticle EoS for two light quark flavours ($m_{u,d} = 0$) and a heavier strange quark ($m_s \simeq 170$ MeV) to describe the plasma phase of an EoS qp.

The quasiparticle model is compared to the lattice results in Fig. 1, where pressure and energy density are shown as a function of temperature. The lattice result for pressure [25] is extrapolated to the continuum limit by assuming a 10% correction, i.e., $p_{cont} \approx 1.1 p_{lat}$ [22], whereas the result for energy density is shown without such an extrapolation. When the quark masses in the quasiparticle model are set temperature dependent as in the lattice calculations, $m_q = 0.4T$ (light quarks) and $m_s = 1.0T$ (heavy quark), the lattice pressure is nicely reproduced (PQP, dashed line). When physical quark masses are chosen (EoS qp, thin solid line), the pressure is larger than with temperature dependent masses.

There is no quasiparticle result with temperature dependent masses available for energy density, but comparison of quasiparticle model with physical quark masses (EoS qp) to the lattice shows nice reproduction of the lattice energy density just above T_c but much larger density above $1.5T_c$. This can be partly explained by the missing extrapolation to continuum limit of the lattice result. If one assumes similar 10% correction than for pressure, the difference between lattice and EoS qp is quite similar for both pressure and energy density at high temperature. The parametrized EoS T (see later in the text) is included for comparison's sake and is shown to lead to much larger pressure and energy density than lattice calculations.

4

The large difference between EoS qp and lattice below T_c is intentional and not related to the quasiparticle model. In the present lattice simulations pions turn out too heavy and therefore their contribution to pressure and entropy is strongly suppressed. Thus one may expect the lattice calculations to give too small pressure and entropy density in the hadronic phase below T_c. The quasiparticle model reproduces also this feature of the lattice EoS and one has to describe the hadronic phase using another model.

We adopt the usual approach of using an EoS of noninteracting hadron resonance gas to describe the hadronic phase. It has been shown that such an EoS describes interacting hadron gas reasonably well at temperatures around pion mass [26] and that the hadron resonance gas approach reproduces the lattice results below T_c if the same approximations are used in both [27]. The properties of hadron resonance gas depend on the number of particles included in the model. Here we include all the strange and non-strange particles and resonances listed in the Particle data Book up to 2 GeV mass. The details of constructing this EoS can be found in Ref. [28].

To circumvent our ignorance of the behaviour of the EoS around T_c, we use the approach outlined in Ref. [29]: We use the hadron resonance gas EoS up to a temperature $T_c - \Delta T$, the quasiparticle EoS above T_c and interpolate smoothly between these two regimes. In practice we choose the values $T_c = 170$ MeV and $\Delta T = 5$ MeV and connect the entropy densities of both models using a polynomial function. We require that the first, second and third temperature derivatives of entropy density are continuous to approximate a smooth crossover from hadronic to plasma phase. Below $T_c - \Delta T$ we use the hadron resonance gas values for pressure and energy density. Above this limit we obtain $P(T)$ and $\varepsilon(T)$ by using the thermodynamical relations $\mathrm{d}P = s\,\mathrm{d}T$ and $\varepsilon = Ts - P$. This EoS is called EoS qp in the following.

For comparison's sake we also carry out the calculations using the EoS Q and H used in Refs. [10,12,14,15,16]. EoS H is a purely hadronic EoS without any phase transition. It is constructed by extending the previously described hadron resonance gas EoS to arbitrarily high temperatures. EoS Q, on the other hand, is inspired by a bag model and contains a first order phase transition from hadron gas to ideal parton gas. The hadron phase is again described by an hadron resonance gas and the plasma phase by a gas of ideal massless quarks and gluons with a bag constant. To approximate the effect of the finite strange quark mass we use the number of quark flavours $N_f = 2.5$. The phase boundary is determined using the Gibbs criterion $p_{\mathrm{HG}}(T_c) = p_{\mathrm{QGP}}(T_c)$ and the two phases are connected using the Maxwell construction at $T_c = 165$ MeV. Details of constructing these two EoSs can be found in Ref. [28].

As can be seen in Fig. 2 the quasiparticle and bag model inspired EoSs (qp and Q, respectively) lead to quite different behaviour around critical tem-
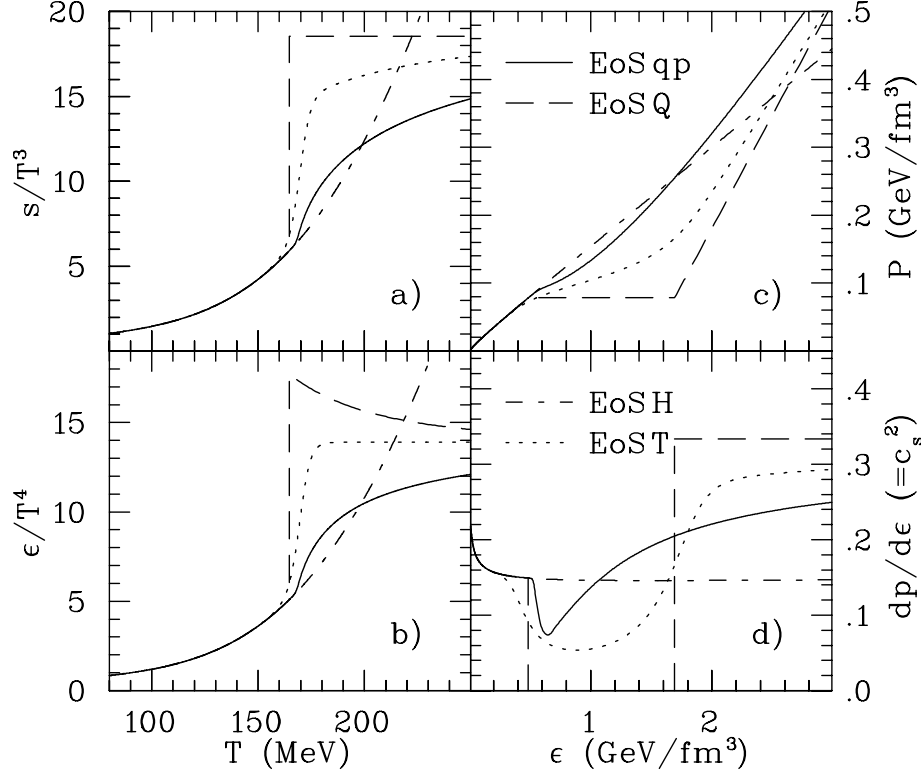
Fig. 2. (a) The entropy density divided by T^3 and (b) the energy density divided by T^4 as functions of temperature, (c) the pressure and (d) velocity of sound squared as functions of energy density in the EoSs qp (quasiparticle EoS), Q (ideal parton gas with first order phase transition), H (hadron resonance gas) and T (ansatz with crossover).

perature. Since we want to study the effects of the order of phase transition and slow approach to ideal Stefan-Boltzmann values separately, we construct yet another EoS. We follow the idea presented in Ref. [20] and connect the hadron and parton phases of the EoS by a hyperbolic tangent function. We refine this approach by using hadron resonance gas EoS instead of ideal pion gas to describe the hadron phase. In Ref. [20] the entropy densities of hadron and parton phases are connected in this way. This leads to similar behaviour of energy density than the Maxwell construction of EoS Q — above T_c energy density rises above the ideal Stefan-Boltzmann limit and approaches the ideal values from above. There is no sign of this kind of behaviour in the lattice results. Therefore we use hyperbolic tangent to connect the energy density of the different phases instead of entropy density. Energy density is given by

$$\varepsilon(T) = \frac{1}{2}\left[\varepsilon_{\mathrm{HRG}}(T)\left(1 - \tanh\frac{T - T_c}{\Delta T}\right) + \frac{169}{120}\pi^2 T^4\left(1 + \tanh\frac{T - T_c}{\Delta T}\right)\right] \quad (1)$$

where the latter term is the energy density of ideal parton gas with 3 colours and 2.5 quark flavours. We use again $T_c = 170$ MeV and make the crossover rapid by choosing $\Delta T = 5$ MeV. After obtaining $\varepsilon(T)$ we again use standard

thermodynamical relations, $(\partial S/\partial E)_{N,V} = 1/T$ and $P = Ts - \varepsilon$, to obtain entropy density and pressure as a function of temperature. This EoS is called EoS T in the following.

All four EoSs are compared in Fig. 2 where entropy and energy density are shown as functions of temperature and pressure and the square of the speed of sound are shown as functions of energy density for each EoS. As can be seen the behaviour of the lattice inspired EoS qp is quite different from the previously used EoS Q with a first order phase transition. The latter has a relatively large latent heat of 1.15 GeV/fm^3 whereas in the former the region where the speed of sound is small and the EoS soft is much smaller. The parametrised EoS T is a compromise between these two. It can also be seen that above the phase transition region the EoS Q has the largest speed of sound and is therefore hardest whereas the EoS H without phase transition is softest.

It is worth noticing that EoS qp depicts a smaller rise in both energy and entropy densities around T_c than what could be expected from lattice calculations. This is not a property of the quasiparticle model used here, but due to the use of hadron resonance gas EoS below T_c. As mentioned before, lattice calculations lead to too high pion mass and correspondingly too small densities below T_c. If realistic pion masses are used in hadron resonance gas, its pressure and densities are well above lattice results below T_c.

3 Initialization

We use the same boost-invariant hydrodynamic code than in Refs. [14,15,16] and described in detail in Ref. [30]. To fix the parameters of the model, we require that the model reproduces the p_T spectra of pions and net protons $(p - \bar{p})$ in most central collisions and the centrality dependence of pion multiplicity at midrapidity. We use net protons instead of protons and/or antiprotons because our model assumes chemical equilibrium to hold down to kinetic freeze-out temperature and is unable to reproduce proton and antiproton yields simultaneously.

Some parametrisations to fix the initial density distributions were explored in Ref. [16]. None of them reproduces the observed centrality dependence of multiplicity, but a linear combination of them does. Here we use the same combination than in Refs. [10,12]. The local entropy density is taken to scale with a linear combination of the density of participants and binary collisions in the transverse plane with weights of 0.75 and 0.25, respectively. This kind of scaling can be interpreted as particle production from "soft" and "hard" processes. For the sake of simplicity, the initial baryon number density is taken

to scale with the number of participants. The initial time of the calculation, $\tau_0 = 0.6$ fm/c, is taken from earlier calculations for $\sqrt{s_{\mathrm{NN}}} = 130$ GeV energy [14,15].

The freeze-out energy density is chosen to reproduce the slopes of pion and net proton spectra in most central collisions (see upper left panel of Fig. 3). The stiffer the EoS, the sooner, i.e. at higher density, the necessary flow velocity to fit the spectra has been built up. We find that effectively the EoS qp is stiffest since it requires the highest decoupling energy density $\varepsilon_{fo} = 0.14$ GeV/fm^3 ($\langle T_{fo} \rangle = 141$ MeV) to fit the data. Even if the ideal parton gas EoS is stiff, the mixed phase of the EoS Q makes it effectively the softest EoS here. The stiffening of the phase transition region and softening of the plasma phase in the EoS T cancel each other. It is almost as soft as EoS Q and can use the same freeze-out energy density $\varepsilon_{fo} = 0.08$ GeV/fm^3 ($\langle T_{fo} \rangle = 130$ MeV). The purely hadronic EoS H is in between these extremes and requires $\varepsilon_{fo} = 0.10$ GeV/fm^3 ($\langle T_{fo} \rangle = 135$ MeV) to fit the data. As can be seen in the upper left panel of Fig. 3, these choices of ε_{fo} allow all EoSs to fit the data equally well.

4 Results

4.1 p_T-spectra

The transverse momentum spectra for pions, kaons and net protons for various centralities are shown in Fig. 3. Pion and net proton spectra in most central collisions were used to fix the parameters of the model, but the data are well reproduced at other centralities too. Only at the most peripheral collisions the data tend to favour flatter spectra than calculated.

The kaon spectra was not taken into account when choosing the parameters and the calculated spectra is a prediction in most central collisions too. The fit to data is surprisingly good when one takes into account that the freeze-out temperature is well below the $T_{\mathrm{chem}} \approx 174$ MeV chemical freeze-out temperature where particle yields are fixed [23].

The net proton spectra is well reproduced up to $p_T = 2.5$ - 3.0 GeV except in the most peripheral collisions, where the data begins to deviate form the calculation at lower p_T. It is worth noticing that we are able to fit the p_T spectra of net protons without any initial transverse velocity field whereas the fit of protons in Ref. [19] required a non-zero initial transverse velocity. One reason for this is that due to larger errors, it is easier to fit the net-proton than proton spectra. The main cause is, however, the different EoS in the hadronic phase. In [19], the authors assumed a separate thermal and kinetic freeze-outs and
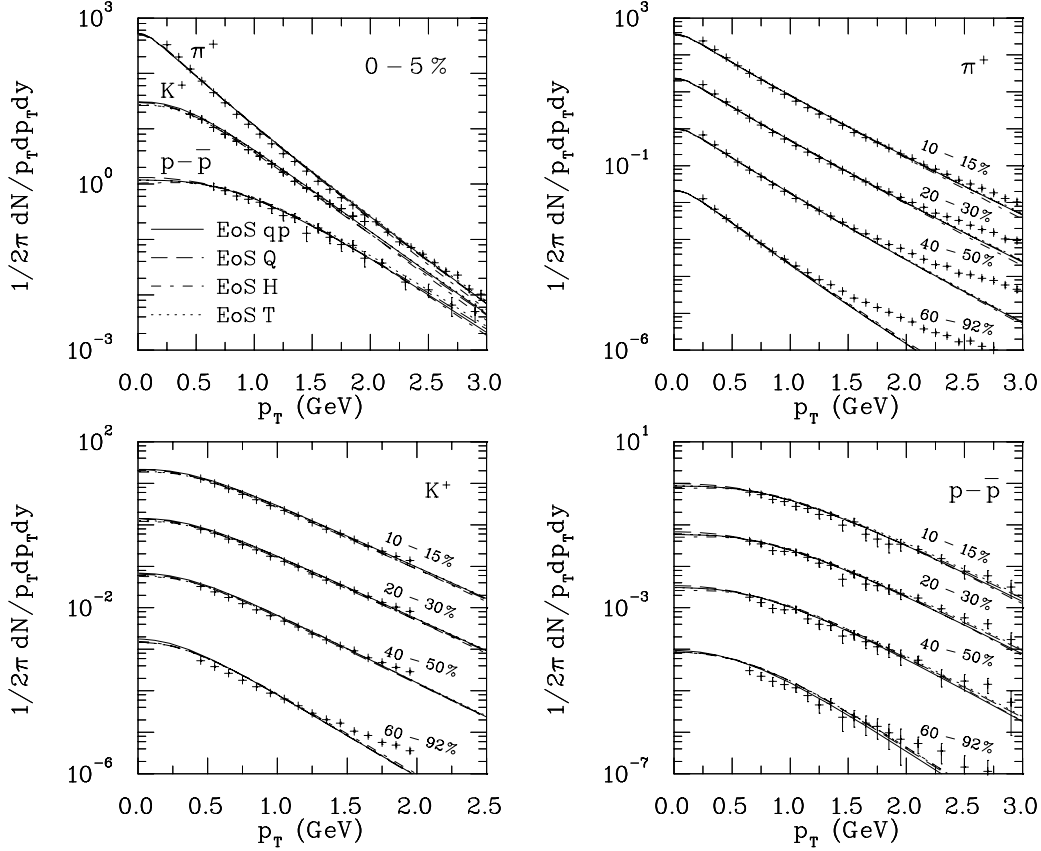
8

Fig. 3. Pion (π^+), kaon (K^+) and net proton ($p-\bar{p}$) p_T-spectra in most central (top left) and semi-central to peripheral Au+Au collisions at $\sqrt{s_{AA}} = 200$ GeV compared with hydrodynamical calculations using four different EoSs. The data was taken by the PHENIX collaboration [31]. For clarity the spectra at centralities 20 - 30%, 40 - 60% and 60 - 80% are scaled by factors 10^{-1}, 10^{-2} and 10^{-3}, respectively.

only a partial chemical equilibrium in the hadronic phase whereas in this work a full chemical equilibrium is assumed. Although the relation between pressure and energy density is almost independent of these assumptions, the relation between temperature and energy density depends strongly on them [18,32]. Thus the relation between collective and thermal motion in a hydrodynamical model depends on the assumption of chemical equilibrium or non-equilibrium and very different initial states can be required to fit the data.

4.2 Elliptic anisotropy

The second Fourier coefficient, v_2, of the azimuthal distribution of charged particles as function of centrality is shown as a histogram in Fig. 4. Note that the data measured by the STAR [6] and PHENIX [1] collaborations have different pseudorapidity and p_T cuts. After these cuts have been applied to the calculations, the results differ slightly. Therefore the comparison with the
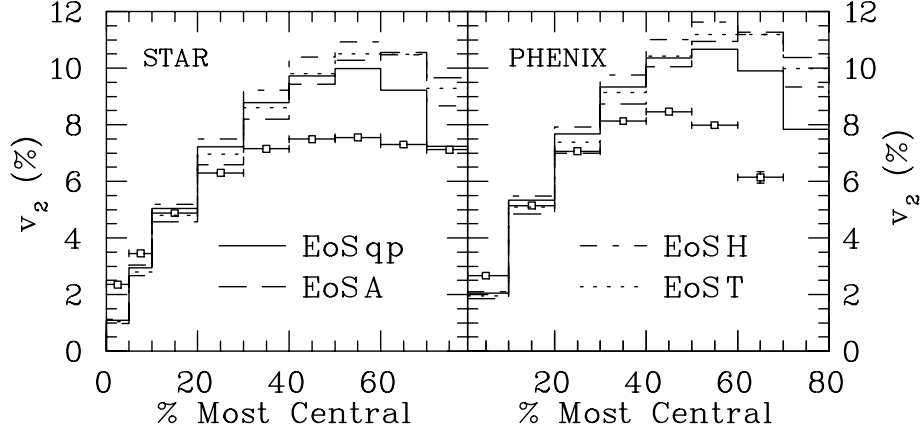
Fig. 4. Centrality dependence of elliptic flow of charged hadrons calculated using three different equations of state and compared with data by the STAR [6] and the PHENIX [1] collaborations. The STAR data is for $|\eta| < 1.2$ and $p_T > 0.15$ GeV and the PHENIX data is for $|\eta| < 0.35$ and $0.2 < p_T < 10$ GeV. The same cuts have been applied to the hydrodynamic calculations.

data is done in two separate panels. The agreement with data is similar to that seen in $\sqrt{s_{\mathrm{NN}}} = 130$ GeV collisions [11,14,33]: at most central collisions ($< 10\%$ of cross section, $b \lesssim 4.6$ fm) the observed anisotropy is above the hydrodynamical result. At semicentral collisions the calculations fit the data (10 - 30% of cross section, $4.6 \lesssim b \lesssim 8$ fm, depending on the EoS) and at peripheral collisions the calculated anisotropy is well above the observed. One possible explanation for larger observed than calculated anisotropy in most central collisions is fluctuations in the initial state geometry [34]. The present experimental procedure cannot distinguish between the enhancing and suppressing effects of fluctuations on anisotropy in most central collisions and consequently leads to too large value of v_2.

The sensitivity of the anisotropy to the EoS depends on centrality. In the most central and semi-peripheral collisions EoS Q leads to the lowest anisotropy and EoS H to the largest, but in most peripheral collisions the lowest anisotropy is achieved using EoS qp. The stiffest EoS does not always lead to the largest anisotropy and the softest to smallest because of the interplay of collective and thermal motion. Stiff EoS may necessitate decoupling at higher temperature when larger thermal motion dilutes the flow anisotropy.

The momentum dependence of elliptic flow, $v_2(p_T)$, in minimum bias collisions is shown in Fig. 5 for positive pions and antiprotons and in Fig. 6 for neutral kaons and a sum of lambdas and antilambdas. For pions the behaviour is similar to the charged particle $v_2(p_T)$ at $\sqrt{s_{\mathrm{NN}}} = 130$ GeV collisions [12,14]. Regardless of the EoS the calculated anisotropy reproduces the data up to $p_T \approx 1.5$ GeV where the data begins to saturate but the hydrodynamical curve keeps increasing. Major differences between different EoSs are at the high p_T region where no EoS fits the data. Closer look at low p_T region ($p_T < 1$ GeV)
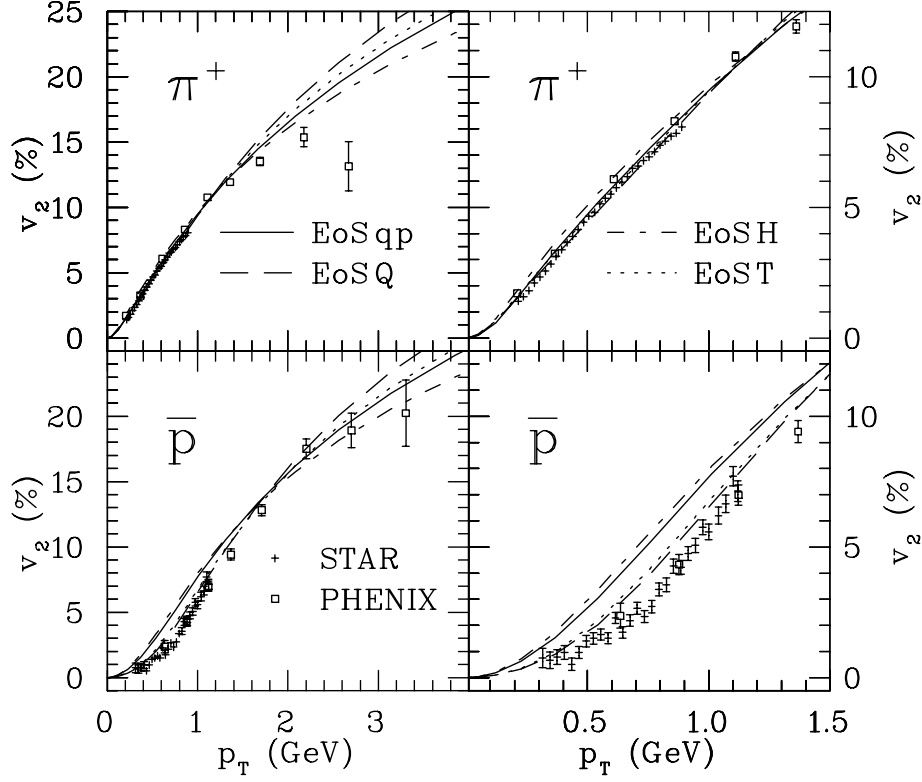
10

Fig. 5. Elliptic flow of pions and anti protons vs. transverse momentum in minimum bias Au+Au collisions at $\sqrt{s_{NN}} = 200$ GeV calculated using four different EoSs and compared with the data by the STAR [3] and PHENIX [1] collaborations. Feed-down from weak decays of strange baryons is included in the calculations.

reveals that EoS H leads to slightly larger v_2 than the other EoSs, but the difference is equal to the difference between the STAR and PHENIX data.

The antiprotons show much stronger sensitivity to the EoS than pions. Below $p_T = 2$ GeV the results form two groups. EoSs qp and H lead to almost identical $v_2(p_T)$ which is clearly above the data whereas EoSs Q and T lead to anisotropy very close to the data. The phase transition crossover in EoS T is very rapid with $\Delta T = 5$ MeV. We have tested that increase in ΔT leads to larger antiproton $v_2(p_T)$ at low p_T and worse fit with the data. For example $\Delta T = 17$ MeV moves the $v_2(p_T)$ curve roughly halfway between results for EoS Q and qp. At high values of p_T the order of results is changed with EoS Q leading to highest and EoS H to the lowest anisotropy. The antiproton data follows the hydrodynamical calculation to much higher values of p_T than the pion data. Even the highest data point at $p_T = 3.2$ GeV is fitted while using EoS qp or H.

Even when EoS Q is used, we can not reproduce the antiproton $v_2(p_T)$ as well as in earlier studies [15]. The main reason is that in Ref. [15] freeze-out temperature was lower $T_f \approx 120$ MeV, but after constraining the freeze-out to fit the p_T spectra we are forced to use higher freeze-out temperature which
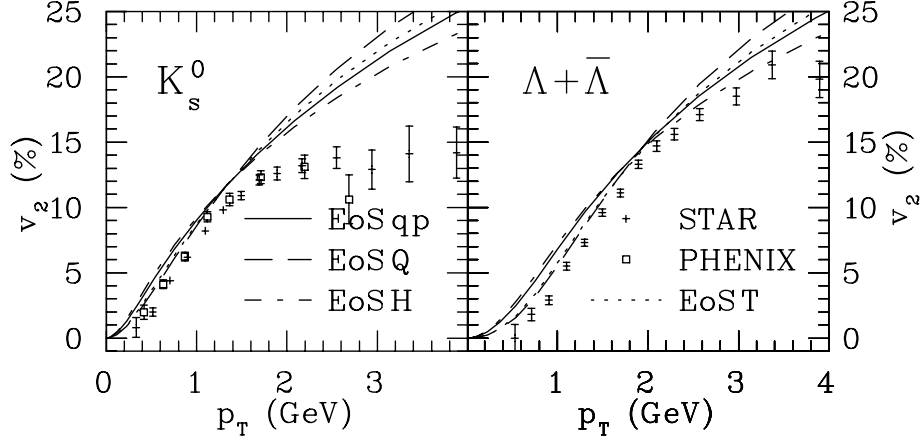
11

Fig. 6. Elliptic flow of kaons and lambdas vs. transverse momentum in minimum bias Au+Au collisions at $\sqrt{s_{NN}} = 200$ GeV calculated using four different EoSs and compared with the data by the STAR [3] and PHENIX [1] collaborations.

does not allow as good description of the v_2 data.

The general behaviour of antiproton $v_2(p_T)$ suggests that the larger the latent heat, the smaller the $v_2(p_T)$ at low p_T. However, this is not the case. To test this hypothesis we used also an EoS with a first order phase transition and larger latent heat than EoS Q (2 GeV/fm^3 instead of 1.15 GeV/fm^3). The fit to antiproton anisotropy was no better than for EoS Q (similar behaviour was already seen in Ref. [11] for EoSs with latent heats 0.8 and 1.6 GeV/fm^3).

Comparison with the strange particle data (K_s^0, $\Lambda + \bar{\Lambda}$) in Fig. 6 shows similar trends. The larger the particle mass the larger the differences between EoSs at low p_T. The data deviates from the overall behaviour of hydrodynamical calculation at lower p_T for mesons than for baryons – the kaon data deviates already around $p_T \approx 1.2$ GeV whereas hydrodynamical calculation is close to lambda data up to $p_T \approx 3.5$ GeV. On the other hand the overall fit to data is worse for strange than non-strange particles. Even EoS Q leads to calculated anisotropy which is above the data also at low p_T. Smaller v_2 at low p_T can not be interpreted as a sign of strange particles freezing out earlier at higher temperature. For kaons and lambdas that would mean *larger* v_2 at small p_T. The good fit to kaon p_T spectra is also against a higher kinetic freeze-out temperature for strange particles.

As shown in Ref. [16], the different parametrisations of the initial state can lead to similar pion $v_2(p_T)$ but different proton $v_2(p_T)$ in minimum bias collisions. We have checked if it would be possible to bring the antiproton $v_2(p_T)$ down to fit the data using EoS H but different initial state as speculated in Ref. [8]. To do this we assumed that at each value of impact parameter b, the initial energy density was proportional to the density of binary collisions in the transverse plane (parametrisation eBC of Ref. [16]), but the proportionality constant depended on impact parameter to reproduce the observed centrality
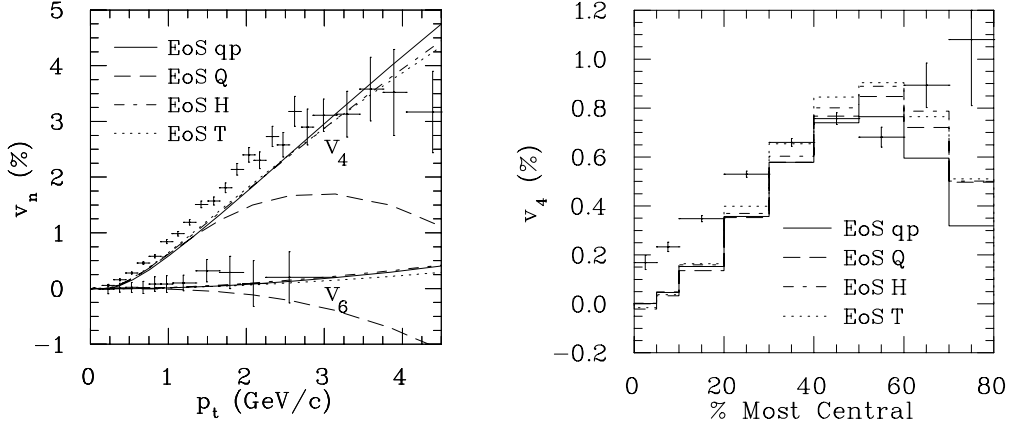
Fig. 7. The fourth and sixth harmonics, $v_4(p_T)$ and $v_6(p_T)$, in minimum bias collisions (left) and p_T-averaged fourth harmonic, v_4, of the azimuthal distribution of charged hadrons as function of centrality (right) calculated using four different EoSs and compared with the STAR data [6].

dependence of multiplicity. Because this parametrisation led to steeper initial gradients than our usual parametrisation, we had to use freeze-out energy density $\varepsilon_f = 0.12$ GeV/fm^3 instead of $\varepsilon_f = 0.1$ GeV/fm^3 ($\langle T_f \rangle = 138$ MeV and $\langle T_f \rangle = 135$ MeV, respectively) to reproduce the p_T distributions of pions and net-protons. As a result, the earlier decoupling negated the change due to the different initial shape and the final proton $v_2(p_T)$ was almost similar to that shown in Fig. 5 and well above the data. We conclude that the anisotropies shown in Figs. 5 and 6 are typical for each EoS and robust against small variations in the initial parametrisation of the system.

4.3 Higher harmonics

Recently there has been interest in measuring the higher harmonics of the azimuthal distribution of particles [3,6]. It has been proposed that these higher coefficients should be even more sensitive to the initial configuration of the system than the elliptic flow coefficient v_2 [7]. A detailed study of these coefficients would require checking how different initial configurations would affect these coefficients. Instead we calculate the fourth and sixth harmonics of distribution, v_4 and v_6, using the initial state defined above as a first attempt to see how an EoS affects higher harmonics.

The fourth and sixth harmonics of the charged particle distribution in minimum bias collisions, $v_4(p_T)$ and $v_6(p_T)$ as function of transverse momenta are shown in the left panel of Fig. 7. The EoS has significant effect only above $p_T \approx 2$ GeV, i.e. in the region where $v_2(p_T)$ is no longer reproduced by hydrodynamics. EoS Q leads to v_4 peaking around $p_T \approx 3$ GeV whereas all the other EoSs lead to monotonous increase of $v_4(p_T)$ with increasing p_T. The data, on the other hand, increases up to $p_T \approx 3$ GeV and saturates. Except
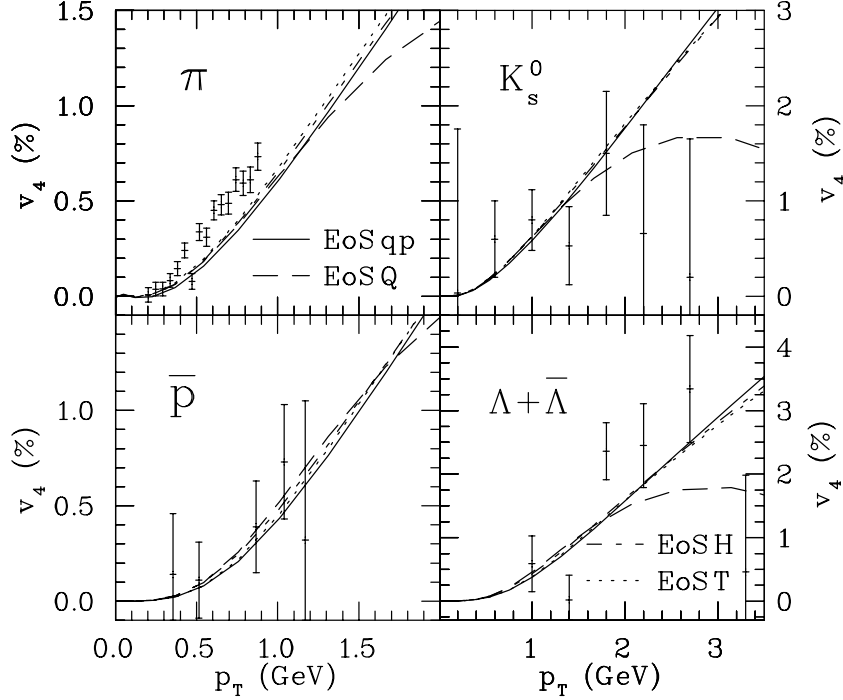
13

Fig. 8. The fourth harmonic, $v_4(p_T)$, of the azimuthal particle distribution of pions, anti-protons, K_S^0 and $\Lambda + \bar{\Lambda}$ for minimum bias Au+Au collisions calculated using four different EoSs and compared with the preliminary STAR data [3].

for the high p_T region all the EoSs lead to v_4 which is smaller than the experimentally measured values. The measured values of the sixth harmonics of the distribution, v_6, are consistent with zero, although the errors are large enough not to exclude any of the calculations here. The calculated values of v_6 are also small but show a qualitative dependence on the EoS: EoS Q leads to negative v_6 whereas all the other EoSs lead to positive values of v_6.

The centrality dependence of the p_T averaged fourth harmonic v_4 is shown in the right panel of Fig. 7. It shows qualitatively similar behaviour to $v_4(p_T)$. The EoS has only a weak effect on v_4 except in peripheral collisions. In central and semicentral collisions the calculated values are below the observed ones.

In Fig. 8 the p_T dependence of fourth harmonic v_4 in minimum bias collisions is shown for identified pions, kaons (K_s^0), antiprotons and lambdas. As was the case for charged hadrons, the EoS has only a weak effect on results below $p_T \approx 2$ GeV. The pion data is above the hydrodynamical calculations. The errors for other particles are large and the calculations fit the data except at the highest p_T where kaon data seems to favour EoS Q and lambda data all the other EoSs.

14

	EoS qp	EoS Q	EoS H	EoS T
$\langle T_{fo} \rangle$ (MeV)	141	130	134	130
$\langle v_r \rangle$	0.47	0.47	0.49	0.49
ϵ_x	0.058	0.033	0.056	0.034
a_2	0.027	0.027	0.025	0.026

Table 1
Freeze-out temperature, average transverse flow velocity, spatial eccentricity and flow anisotropy on the decoupling surface in Au+Au collision with impact parameter $b = 6$ fm using four different EoSs.

5 Flow on decoupling surface

To understand how different EoSs lead to different anisotropies, we study the properties of the freeze-out surface in Au+Au collision with impact parameter $b = 6$ fm. We try to find a set of parameters to describe the surface similar to those presented in Ref. [35] for a blast wave model. Freeze-out temperature, average transverse flow velocity and two anisotropy coefficients are shown in Table 1. To characterise the spatial anisotropy of the surface we generalise the usual spatial anisotropy ϵ_x [30] for hypersurfaces:

$$\epsilon_x = \frac{\int \partial_\mu s^\mu \left(y^2 - x^2 \right)}{\int \partial_\mu s^\mu \left(y^2 + x^2 \right)}, \tag{2}$$

where the usual integral over $\mathrm{d}x\,\mathrm{d}y$ is replaced by an integral over space-time hypersurface and instead of energy density, entropy density is used as a weight. To characterise the azimuthal modulation of the flow field, we first calculate average flow velocity as function of flow angle, $\langle v_r(\phi_v) \rangle$, where $\phi_v = \arctan(v_y/v_x)$. We use the second Fourier coefficient of this distribution as a measure of anisotropy of the flow field:

$$a_2 = \frac{\int \mathrm{d}\phi \, \langle v_r(\phi) \rangle \, \cos(2\phi)}{\int \mathrm{d}\phi \, \langle v_r(\phi) \rangle}. \tag{3}$$

This allows us to separate the spatial anisotropy from the flow anisotropy.

The average flow velocity and anisotropy of the velocity field are surprisingly similar in all four cases. The main differences at freeze-out are freeze-out temperature and the shape of the surface. As seen in Ref. [36] where the anisotropies are studied using a parametrisation of the freeze-out surface, at this temperature and velocity range the lower temperature should lead to larger anisotropies for both pions and protons. As can be expected, in parametrisation smaller spatial anisotropy is seen to lead to smaller v_2 of par-
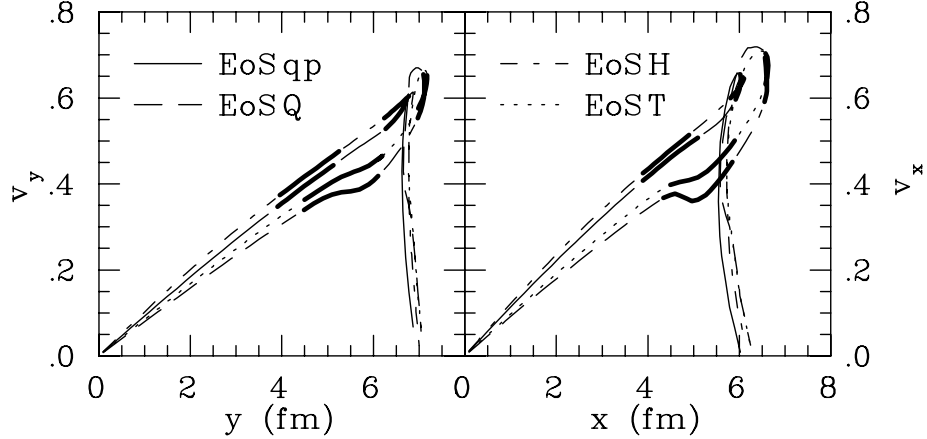
Fig. 9. The transverse flow velocity on decoupling surface of a Au+Au collision with impact parameter $b = 6$ fm using four different EoSs. The left panel shows the velocity as function of y-coordinate when $x = 0$ and the right panel as function of x when $y = 0$. The curves are divided into segments of thin and thick lines where each segment corresponds to 20% of total entropy flowing through freeze-out surface.

ticles. This behaviour is different from what we see here where EoS Q leads to lowest $v_2(p_T)$ at low p_T. Smaller spatial anisotropy can not explain this alone, since its effect should be cancelled by lower temperature. Also the differences between EoS Q and T are such that one would expect EoS T to lead to lower v_2 for both pions and protons, but that is not the case.

Clearly the average values do not characterise the flow well enough. The reason for different anisotropies must lie in the details of the flow profiles. To have a closer look at the properties of flow on the decoupling surface, we have plotted the flow velocity on decoupling surface as a function of radial coordinate in Fig. 9. In the left panel the flow velocity is shown as function of y when $x = 0$ and in the right panel as function of x when $y = 0$.

As expected from very similar spectra and differential anisotropies, the velocity distribution for EoSs qp and H is also close to each other. EoS Q, on the other hand, leads to different flow profile with slower increase of velocity with increasing radius, a distinctive "shoulder" at $r \approx 5$ fm where the velocity can even slightly decrease with increasing r (in x-direction) and very rapid rise of flow velocity close to maximum radius of the system. EoS T on the other hand is somewhere in between these two with the slow rise at low r and very rapid rise at large r but with much weaker structure around $r \approx 5$ fm.

Even if the flow velocity distributions shown in Fig. 9 do not look too different from each other, the amount of particles emitted from fluid elements at different velocities is very different. To characterise this, the velocity curves in Fig. 9 are divided into segments so that each segment corresponds to 20% of entropy flowing through surface and thus $\sim 20\%$ of particles emitted. Also the entropy flow as function of flow velocity on the decoupling surface is shown in Fig. 10.
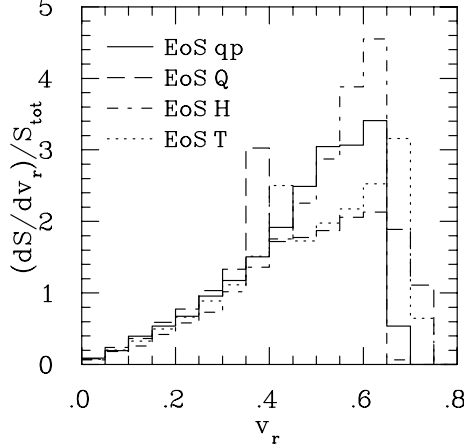
16

Fig. 10. Entropy flow through fluid elements on decoupling surface as function of the transverse flow velocity of each fluid element.

As can be seen EoS Q leads to very different distribution with much more particles being emitted at small flow velocities. Especially the "shoulder" in flow profile around $r = 5$ fm leads to a peak in entropy distribution at $v_r \approx 0.38$ whereas EoSs qp and H lead to distributions peaking at $v_r \approx 0.6$, close to maximum values of flow velocity. EoS T is again a compromise between these two extremes. The entropy flow has a peak both at the "shoulder" at $v_r \approx 0.42$ and close to maximum velocity at $v_r \approx 0.68$. The largest flow velocity is also larger than for EoSs qp and H and close to the maximum for EoS Q. The flow on decoupling surface is thus weighted very differently for each EoS and the average values of flow velocity and anisotropy do not completely describe p_T differential anisotropies of particles.

In Ref. [11] similar velocity profiles were considered linear and corroborating the general use of linear velocity profiles in hydrodynamically inspired fits to particle spectra. As seen here the deviations from linear behaviour are important at least in non-central collisions. Thus the parameter values from fits can deviate from values obtained in full-fledged hydrodynamical calculations.

6 Conclusions

In this paper we have examined how the order of deconfinement phase transition affects the anisotropy in a hydrodynamical description of relativistic nuclear collision. We used four different Equations of State – one lattice inspired EoS with a crossover transition from hadronic to partonic phase (EoS qp), one where a simple Maxwell construction between different phases creates a first order phase transition (EoS Q), a purely hadronic EoS with no phase transition at all (EoS H) and an EoS where different phases were smoothly connected with a hyperbolic tangent function (EoS T).

17

The p_T distributions of various particles could be reproduced equally well using each of these EoSs when the freeze-out density was chosen accordingly. Our result is thus different from Ref. [11] where p_T distributions were sensitive to the amount of latent heat of the EoS. This difference is due to different treatment of freeze-out. In Ref. [11], the hadronic stage was described using RQMD cascade model which does not have freeze-out temperature or density as a free parameter.

The main sensitivity to the EoS was seen in the differential anisotropy of heavy particles at low p_T, i.e. antiprotons and lambdas. None of the EoSs was able to reproduce the data, but the EoS with the first order phase transition, EoS Q was closest. Surprisingly the lattice based EoS qp was as far from the proton v_2 data as the EoS H without any phase transition. The basic rule was that the sharper the rapid rise in entropy and energy density at phase transition and the larger the latent heat, the lower the differential anisotropy of antiprotons at low p_T was. This, however, is valid only among the EoSs discussed here.

The results here favour EoS Q and first order phase transition over lattice inspired EoS qp. One should not interpret this to mean that hydrodynamical description of elliptic flow requires a first order phase transition since EoS T with a crossover transition lead to only marginally worse results than EoS Q. The main difference between EoSs qp and T is in the size of the increase in energy and entropy densities around the critical temperature and consequently how wide is the region where the speed of sound is small. Thus the acceptable description of elliptic flow seems to require very fast and sufficiently large increase in entropy and energy densities around T_c.

However, these results must be taken as only preliminary. For simplicity hadron gas was assumed to maintain chemical equilibrium until kinetic freeze-out in these calculations. As mentioned in section 3, this assumption does not allow the reproduction of observed particle yields but only the slopes of their spectra and approximatively their anisotropies [10,14]. The recent calculations where this assumption is relaxed and a separate chemical and kinetic freeze-outs included in the model [18,19], have lead to much worse description of the data [37]. It looks like it is very difficult to describe the data using ideal fluid hydrodynamics while the hadron gas is not in chemical equilibrium [38]. On the other hand, if the hadronic phase is described using RQMD cascade which allows chemical non-equilibrium, the data is again reproduced [11]. Thus the correct treatment of the hadronic phase in a hydrodynamical model is an open question and it is not yet possible to draw final conclusions about the details of the EoS based on the observed anisotropies.

Nevertheless our results point to that a large and rapid increase in densities around critical temperature is necessary in hydrodynamical description to describe the observed anisotropies. The failure of lattice inspired EoS to do this

raises the questions whether the lattice result used here is sufficiently accurate around T_c, whether the hadron resonance gas description of the EoS below T_c is inaccurate or whether some finite size effects make the EoS relevant for heavy ion collisions differ from lattice QCD results.

Acknowledgements

References

[1] S. S. Adler *et al.* [PHENIX Collaboration], Phys. Rev. Lett. **91** (2003) 182301 [arXiv:nucl-ex/0305013].

[2] B. B. Back *et al.* [PHOBOS Collaboration], arXiv:nucl-ex/0407012.

[3] J. Adams *et al.* [STAR Collaboration], arXiv:nucl-ex/0409033.

[4] For reviews see, e.g., J. Ollitrault, Nucl. Phys. A **638**, 195 (1998) [arXiv:nucl-ex/9802005]; A. M. Poskanzer, arXiv:nucl-ex/0110013; or S. A. Voloshin, Nucl. Phys. A **715**, 379 (2003) [arXiv:nucl-ex/0210014].

[5] H. Sorge, Phys. Rev. Lett. **78** (1997) 2309 [arXiv:nucl-th/9610026].

[6] J. Adams *et al.* [STAR Collaboration], Phys. Rev. Lett. **92** (2004) 062301 [arXiv:nucl-ex/0310029]; A. M. Poskanzer [STAR Collaboration], J. Phys. G **30** (2004) S1225 [arXiv:nucl-ex/0403019].

[7] P. F. Kolb, Phys. Rev. C **68** (2003) 031902 [arXiv:nucl-th/0306081].

[8] P. Huovinen, in Quark-Gluon Plasma 3, eds. R. C. Hwa and X. N. Wang (World Scientific, Singapore, 2004) [arXiv:nucl-th/0305064].

[9] P. F. Kolb and U. Heinz, in Quark-Gluon Plasma 3, eds. R. C. Hwa and X. N. Wang (World Scientific, Singapore, 2004) [arXiv:nucl-th/0305084].

[10] U. W. Heinz and P. F. Kolb, Nucl. Phys. A **702** (2002) 269 [arXiv:hep-ph/0111075].

[11] D. Teaney, J. Lauret and E. V. Shuryak, arXiv:nucl-th/0110037.

[12] U. W. Heinz and P. F. Kolb, arXiv:hep-ph/0204061.

[13] F. Karsch and E. Laermann, in Quark-Gluon Plasma 3, eds. R. C. Hwa and X. N. Wang (World Scientific, Singapore, 2004) [arXiv:hep-lat/0305025].

[14] P. F. Kolb, P. Huovinen, U. W. Heinz and H. Heiselberg, Phys. Lett. B **500** (2001) 232 [arXiv:hep-ph/0012137].

[15] P. Huovinen, P. F. Kolb, U. W. Heinz, P. V. Ruuskanen and S. A. Voloshin, Phys. Lett. B **503** (2001) 58 [arXiv:hep-ph/0101136].

[16] P. F. Kolb, U. W. Heinz, P. Huovinen, K. J. Eskola and K. Tuominen, Nucl. Phys. A **696** (2001) 197 [arXiv:hep-ph/0103234].

[17] T. Hirano, Phys. Rev. C **65** (2002) 011901 [arXiv:nucl-th/0108004].

[18] T. Hirano and K. Tsuda, Phys. Rev. C **66** (2002) 054905 [arXiv:nucl-th/0205043];

[19] P. F. Kolb and R. Rapp, Phys. Rev. C **67** (2003) 044903 [arXiv:hep-ph/0210222].

[20] J. P. Blaizot and J. Y. Ollitrault, Phys. Rev. D **36** (1987) 916.

[21] D. H. Rischke and M. Gyulassy, Nucl. Phys. A **597** (1996) 701 [arXiv:nucl-th/9509040].

[22] R. A. Schneider and W. Weise, Phys. Rev. C **64** (2001) 055201 [arXiv:hep-ph/0105242].

[23] P. Braun-Munzinger, D. Magestro, K. Redlich and J. Stachel, Phys. Lett. B **518** (2001) 41 [arXiv:hep-ph/0105229].

[24] G. Boyd, J. Engels, F. Karsch, E. Laermann, C. Legeland, M. Lutgemeier and B. Petersson, Nucl. Phys. B **469** (1996) 419 [arXiv:hep-lat/9602007].

[25] F. Karsch, E. Laermann and A. Peikert, Phys. Lett. B **478** (2000) 447 [arXiv:hep-lat/0002003]; F. Karsch, Nucl. Phys. A **698** (2002) 199 [arXiv:hep-ph/0103314].

[26] R. Venugopalan and M. Prakash, Nucl. Phys. A **546** (1992) 718.

[27] F. Karsch, K. Redlich and A. Tawfik, Eur. Phys. J. C **29** (2003) 549 [arXiv:hep-ph/0303108].

[28] J. Sollfrank, P. Huovinen, M. Kataja, P. V. Ruuskanen, M. Prakash and R. Venugopalan, Phys. Rev. C **55** (1997) 392 [arXiv:nucl-th/9607029].

[29] T. Renk, R. A. Schneider and W. Weise, Phys. Rev. C **66** (2002) 014902 [arXiv:hep-ph/0201048].

[30] P. F. Kolb, J. Sollfrank and U. W. Heinz, Phys. Rev. C **62** (2000) 054909 [arXiv:hep-ph/0006129].

[31] S. S. Adler *et al.* [PHENIX Collaboration], Phys. Rev. C **69** (2004) 034909 [arXiv:nucl-ex/0307022].

[32] D. Teaney, arXiv:nucl-th/0204023.

[33] P. Huovinen, Nucl. Phys. A **715** (2003) 299 [arXiv:nucl-th/0210024].

[34] M. Miller and R. Snellings, arXiv:nucl-ex/0312008.

[35] C. Adler *et al.* [STAR Collaboration], Phys. Rev. Lett. **87** (2001) 182301 [arXiv:nucl-ex/0107003].

[36] F. Retiere and M. A. Lisa, Phys. Rev. C **70** (2004) 044907 [arXiv:nucl-th/0312024].

[37] K. Adcox *et al.* [PHENIX Collaboration], Nucl. Phys. A **757** (2005) 184 [arXiv:nucl-ex/0410003].

[38] T. Hirano and M. Gyulassy, arXiv:nucl-th/0506049.